Signal-to-Noise Ratio in Doppler Radar System for Heart and Respiratory Rate Measurements

Amy D. Droitcour, *Member, IEEE*, Olga Boric-Lubecke, *Senior Member, IEEE*, and
Gregory T. A. Kovacs, *Fellow, IEEE*

Abstract—A CMOS Doppler radar sensor has been developed and used to measure motion due to heart and respiration. The quadrature direct-conversion radar transceiver has been fully integrated in 0.25-μm CMOS, the baseband analog signal conditioning has been developed on a printed circuit board, and digital signal processing has been performed in MATLAB. The theoretical signal-to-noise ratio (SNR) is derived based on the radar equation, the direct-conversion receiver's properties, oscillator phase noise, range correlation, and receiver noise. Heart and respiration signatures and rates have been measured at ranges from 0.5 to 2.0 m on 22 human subjects wearing normal T-shirts. The theoretical SNR expression was validated with this study. The heart rates found with the radar sensor were compared with a three-lead electrocardiogram, and they were within 5 beats/min with 95% confidence for 16 of 22 subjects at a 0.5-m range and 11 of 22 subjects at a 1.0-m range. The respiration rates found with the radar sensor were compared with those found using a piezoelectric respiratory effort belt, and the respiration rates were within five respirations per minute for 18 of 22 subjects at a 0.5-m range, 17 of 22 subjects at a 1.0-m range, and 19 of 22 subjects at a 1.5-m range.

Index Terms—Biomedical applications of electromagnetic radiation, biomedical monitoring, cardiovascular system, Doppler radar, microwave integrated circuits, respiratory system.

I. INTRODUCTION

NONCONTACT monitoring of human cardiopulmonary activity through clothing and bedding could be a valuable tool in sleep monitoring and home health-care applications. Standard heart and respiration monitors require contact and usually accurate control or placement, which may be impossible or undesirable in many situations where it would be advantageous to measure the heart and respiration rates. With Doppler radar, it is possible to sense chest motion noncontact and through clothing, from which heart and respiration motion signatures can be isolated, and heart and respiration rates can be derived. These radar transceivers operate in the radio and

microwave frequency bands, and they can function at a power below that of many consumer wireless devices so they are very safe.

Microwave Doppler radar has been used to sense physiologic movement since the early 1970s [1]. The original work was done with bulky, heavy, and expensive waveguide components, limiting its use to research environments. Renewed interest in this technology over a last decade resulted in diverse technological solutions including the use of ultra-wideband (UWB) radar [2], nonlinear demodulation [3], separation of multiple subjects [4], and exploitation of circular polarization [5], to mention just a few. Spatial [6], [7] and frequency diversity [8] was also explored for cancellation of unwanted motion. Recent advances in wireless technology and microfabrication have enabled the integration of a Doppler radar transceiver on a printed circuit board [9], [10], and on a single CMOS chip that is compact, lightweight, and inexpensively mass producible [11]–[14]. With smaller and less expensive circuitry, radar measurement of heart and respiration rates could become practical for many applications where electrode and chest-strap monitors cause discomfort or are difficult to apply, including clinical monitoring of neonates [15] and burn victims [16], home monitoring of infants, the elderly or the chronically ill, and astronaut sleep station monitoring. The potential low cost of the fully integrated version and the potential for a very large market makes home monitoring an attractive target. The silicon-based radar chip in this paper is a continuous-wave quadrature direct-conversion Doppler radar transceiver operating at 2.4 GHz. The transceiver has an effective isotropic radiated power below 10 dBm, well below the limit for consumer wireless devices in this band [17].

This paper will provide the first theoretical derivation and experimental validation of signal-to-noise ratio (SNR) in a Doppler radar system for measurement of heart and respiratory rates. The experimental validation was done using the test results on 22 human subjects, and it was shown that experimental results match the theoretical prediction both for heart and respiratory measurements.

II. SNR THEORY

According to Doppler theory, a target with a time-varying position, but no net velocity, will modulate the reflected signal's phase in proportion to the target's position. A stationary person's chest has a periodic movement with no net velocity, and a continuous wave (CW) radar with the chest as the target will receive a signal similar to the signal it transmits, but with its phase modulated by the time-varying chest position. The Doppler radar heart and respiratory motion monitor requires the measurement of a phase modulation at a very
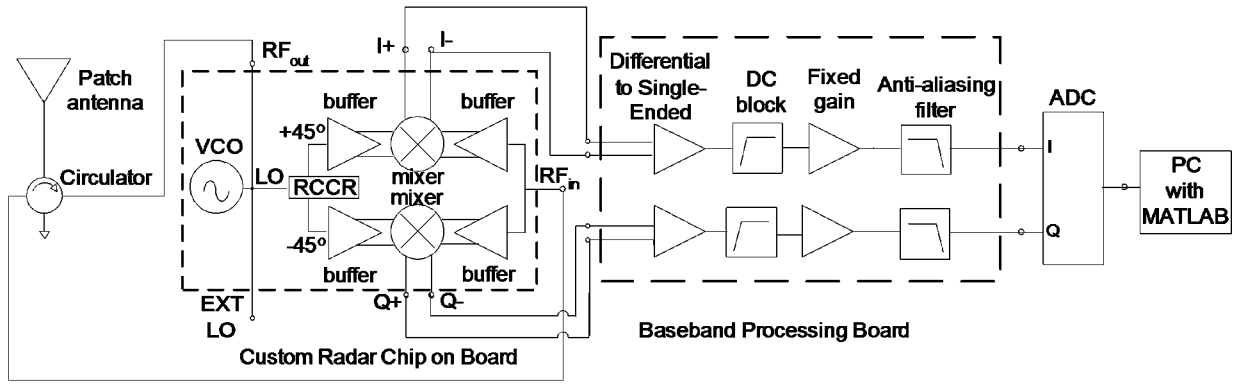
Fig. 1. Block diagram of radar system. The radio transceiver is on the custom radar chip, and a circulator isolates the RF output from the RF input. A single patch antenna is used for both transmitting and receiving. Each baseband channel uses an instrumentation amplifier for single-to-differential conversion, has a dc block and gain stage followed by an antialiasing low-pass filter. The signals are the then digitized and processed with a PC with custom MATLAB signal-processing software.

low offset frequency, and fully integrated CMOS oscillators have high phase noise, which poses a challenging problem. However, in this system, it is possible to take advantage of the range correlation effect because the same oscillator is used for the transmitter and the receiver so the transmitted signal and the local oscillator (LO) have the same phase noise. When a portion of the transmitted signal is reflected from the subject's chest and phase modulated, its phase noise does not change. This means that the received signal has phase noise similar to that of the LO, but shifted in time an amount equal to the signal's round-trip transit time. If the signal's travel time is short compared to the period of the modulations of interest, the phase noise on the received signal is highly correlated with that on the LO, and when the received signal is mixed with the LO, the correlated portion of the phase noise effectively cancels, leaving a much lower level of residual phase noise [12], [18].

The block diagram of the radar system is shown in Fig. 1. The SNR of the radar system at the mixer output depends on a number of parameters, including the oscillator phase noise, mixer $1/f$ noise, and thermal noise. The estimated received power at the mixer output, S_B, is calculated using the radar equation [19], which determines the received power, receiver gain, G_{RX}, mixer conversion loss, G_{CL}, and phase demodulation link equation. The radar equation and link equation calculations are based on the transmitted power P_T, the range to the target R, and the wavelength of the signal λ, the gain of the transmit and receive antenna G, the radar cross section (RCS) of the target σ, and the subject motion $x(t)$

$$S_B = \frac{2P_T G^2 G_{RX} G_{CL} \overline{\sigma x^2(t)}}{4\pi R^4}. \quad (1)$$

There are three main sources of noise: residual phase noise from the oscillator, down-converted RF additive white Gaussian noise (AWGN) from the front end of the receiver, and baseband $1/f$ noise from the mixer and baseband circuits.

A. Residual Phase Noise

The baseband noise spectral density $S_{\Delta\phi}(f_o)$ can be calculated from the RF phase noise spectral density $S_\phi(f_o)$ with the

target at a given range R, offset frequency f_o, and the total delays between the oscillator and the antenna and between the antenna and the receiver, combined as t_d

$$S_{\Delta\phi}(f_o) \approx 2S_\phi(f_o) \left(16\pi \frac{\left(R + \frac{ct_d}{2}\right)}{c^2} \right) \quad (2)$$

where c is the propagation velocity of the signal [18].

The noise power at baseband due to residual phase noise can be derived using the phase modulation link equation with the received RF power from clutter, and assuming the RF phase noise has a -30-dB/decade slope at the offset frequencies of interest. The baseband noise power from residual phase noise is

$$N_{RPN,B} = \frac{P_T G^2 G_{RX} G_{CL} \sigma_c}{\pi f^2} S_\phi(1) \ln\left(\frac{f_{max}}{f_{min}}\right) \frac{\left(R + \frac{ct_d}{2}\right)}{R^2} \quad (3)$$

where f is the RF signal frequency, and f_{max} and f_{min} are the maximum and minimum frequencies of the baseband bandpass filter, σ_c is the RCS of the clutter, and $S_\phi(1)$ is the 1-Hz intercept of the phase-noise spectrum.

B. Baseband $1/f$ Noise

In this application, $1/f$ noise at the mixer output and in baseband signal-conditioning circuits dominates the baseband noise spectrum. Choosing a mixer that minimizes $1/f$ noise, such as a passive mixer, and minimizing the input-referred $1/f$ noise added by the baseband filtering and amplifying stages will minimize the amount of baseband noise. When $1/f$ noise dominates, the baseband receiver noise can be approximated as

$$N_{1/f,B} = \int_{f_{min}}^{f_{max}} P_{1/f}(1)f^{-1}df = P_{1/f}(1)\ln\left(\frac{f_{max}}{f_{min}}\right) \quad (4)$$

where $P_{1/f}$ is the noise power in a 1-Hz bandwidth centered at 1 Hz.

C. AWGN

The dominant RF noise source at the input to the receiver is AWGN. After conversion to baseband, the noise power is

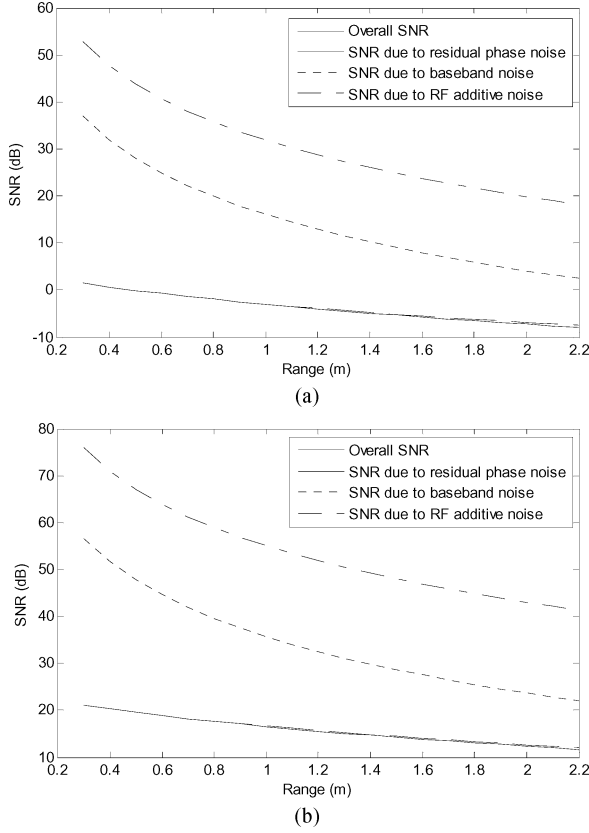$$N_{RF,B} = 8G_{RX} G_{CL}(NF)(kTB). \quad (5)$$

Fig. 2. Theoretical SNR for: (a) heart motion and (b) respiratory motion. Since the residual phase noise is dominant, the overall SNR is nearly identical to the SNR due to residual phase noise.

TABLE I
SYSTEM PARAMETERS USED FOR SNR CALCULATIONS

Symbol	Description	Value
P_T	Transmit power	0 dBm
G	Antenna gain	6 dBi
G_{RX}	Receiver Gain	6 dB
G_{CL}	Conversion Gain	-3 dB
$x^2(t)$	RCS-MSM product (heart)	2.25 mm^4
$x^2(t)$	RCS-MSM product (resp)	500 mm^4
$P_{1/f}(1)$	1/f noise power at 1Hz	-130 dBm/Hz
f_{max}	Maximum frequency - heart	10 Hz
f_{max}	Maximum frequency - resp	10 Hz
f_{min}	Minimum frequency - heart	0.6 Hz
f_{min}	Minimum frequency - resp	0.01 Hz
NF	Receiver noise figure	6 dB
T	RF Noise temperature	300K
t_d	Delay	5ns
$S_\phi(1)$	Phase noise at 1-Hz intercept	64 dB/Hz

of phase noise and baseband noise, the baseband noise dominates over the RF noise, but the residual phase noise dominates over both with the CMOS transceiver. Since the residual phase noise is dominant, the overall SNR is nearly identical to the SNR due to residual phase noise. Equation (6) also indicates that the SNR should be linear with the target RCS, and that the changes in RCS should not affect the dominant type of noise. The RCS for both heart and respiratory motion is expected to vary from subject to subject, and with subject orientation with respect to the antenna.

III. HEART AND RESPIRATION RATE MONITORING SYSTEM

A. Doppler Radar System

For the system developed in this work, the RF radar electronics are on a single CMOS chip and the baseband electronics are on a custom printed circuit board. CMOS chip was mounted on a printed circuit board with dimensions of about 5 cm × 10 cm, and baseband board had dimensions of 9 cm × 11 cm. A commercially available antenna designed for use in the bands of operation was used. Fig. 1 shows a block diagram of the radar system. The microwave portion consists of the on-chip radio transceiver, a circulator, and an antenna.

The antenna used is an Antenna Specialists ASPPT 2988 patch antenna, with a 60° by 80° beamwidth and 8-dBi gain. The antenna is used in conjunction with a Pasternack PE8401 circulator to isolate the received signal from the transmitted signal. The baseband portion of the system consists of two channels, each with a differential-to-single-ended converter followed by a dc-blocking amplification and filtering stage and an antialiasing low-pass filter. Each baseband channel uses a Burr

D. System SNR

Since the noise sources are uncorrelated, when they have been converted to their baseband values, their powers are additive, and thus, the system SNR becomes (6), shown at the bottom of this page. For radar monitoring of heartbeat and respiration, the RCS, the mean-squared motion (MSM), and the clutter cross section are the only values in the SNR expression that change defined with different subjects and environments. The desired RCS–MSM product is actually the integral of the motion over the area of the body, multiplied by factors for the body reflectivity, the directivity of the reflected signal, and the amount of motion that is in the direction of the antenna. The peak-to-peak chest motion due to respiration in adults ranges from 4 to 12 mm [20], [21], while the peak-to-peak motion due to the heartbeat is about 0.5 mm [22].

The calculated SNR is shown in Fig. 2(a) and (b) for heart motion and respiratory motion, respectively, as a function of range, assuming system parameters shown in Table I. These plots indicate that with calculated values of RF noise and measured values

$$\left(\frac{S}{N}\right) = \frac{\sigma \overline{x^2(t)}}{2\pi \frac{(N_{1/f,B} + N_{RF,B})}{P_T G^2 G_{RX} G_{CL}} R^4 + 2\left(\frac{\sigma_c}{f^2} S_\phi(1) \ln\left(\frac{f_{max}}{f_{min}}\right)\right)\left(R + \frac{ct_d}{2}\right)^2}$$

(6)

Brown INA105 precision differential amplifier (Texas Instruments Incorporated, Dallas, TX) and a Texas Instruments Incorporated OPA4132 quad field-effect transistor (FET) input operation amplifier (Texas Instruments Incorporated), provides 40-dB gain, and passes from 0.2 to 20 Hz. A 16-bit National Instruments 6036E NIDAQ PCMCIA card (National Instruments, Austin, TX) was used with a PC for digitization at 100-Hz sampling rate and custom MATLAB software performs digital signal processing (DSP). The baseband board also includes power circuitry so that the board and the CMOS chip can be powered with a single battery. The signal conditioning board operates at ±5, and the CMOS chip operates at 3 V with an oscillator tuning voltage of 3.5 V. A Power-Sonic PS-628 rechargeable lead-acid battery (Powersonic Corporation, Redwood City, CA) was used to power the board.

B. Chip Architecture

A block diagram of the quadrature CMOS microwave radio is shown in Fig. 1. The voltage-controlled oscillator (VCO) provides both the 1-dBm 2.4-GHz RF output signal and the LO signal, and it consumes 40 mW. The oscillator signal is split into the RF output signal that drives the antenna and the LO signal that is used for demodulation. The LO is then split into two quadrature LO signals for in-phase (I) and quadrature (Q) receiver chains. The quadrature LO signals are created with a passive resistor–capacitor–capacitor–resistor (RCCR) network, which provides a $+45°$ phase shift to one LO output and a $-45°$ phase shift to the other output. In each receiver chain, an active balun amplifies the LO signals and converts the single-ended signals to the differential signals required by the double-balanced mixer. Each balun-amplifier dissipates at 15 mW. The RF input signal is passively divided into the two receiver chains, and active balun amplifiers convert single-ended RF signals to differential RF signals that feed the mixer. The double-balanced ring mixer is fully passive; use of a balanced mixer minimizes even-order distortion, which is especially important in a direct-conversion architecture, as even-order distortion creates interference at the baseband signal. Additionally, a passive mixer decreases $1/f$ noise that can be limiting in homodyne systems that have data near dc. This chip consumes a total of 100 mW with a 3-V bias. The chip was fabricated in a 0.25-μm CMOS process with five metal levels, including a 3-mm-thick top-level metal providing an inductor quality factor of 8–10. The chip has a size of 4.3 mm × 3.8 mm and is packaged in the Amkor exposed pad TQFP-48 package (Amkor Technologies, West Chester, PA) with a 7 mm × 7 mm body size.

C. DSP

The DSP filters the signals to remove noise and to isolate the Doppler heart signal from the respiration signal, combines signals from the I and Q channels, determines the rate of the signal, and smooths the output rate. The first DSP step is to isolate the heart signal from the combined heart and respiration signals with a 400-tap Kaiser high-pass filter with β of 6.5 and a cutoff of 0.6 Hz. The heart signals are then low-pass filtered to remove out-of-band noise with a 20-tap Kaiser filter having a β of 6.5 and a 20-Hz cutoff. The I and Q signals are then combined with SVD combining [23]. The delay introduced by the filters

is corrected so the time scale is the same for all channels. The Doppler heart rate is calculated every 0.5 s; the signal in a 8-s Hamming window is autocorrelated, and the local maxima that would indicate a rate between 30–120 beats/min is used to calculate the heart rate. The heart rate from the electrocardiogram is determined by extracting the R waves using a wavelet-based algorithm [24] and inverting the mean of the inter-beat interval (in seconds) in an 8-s window and multiplying by 60 to obtain beats per minute. The rates from both the electrocardiogram (ECG) and the Doppler system are then smoothed with an exponential filter having an α value of 0.93.

The respiration is extracted from the combined heart and respiration signal. The respiration signal is low-pass filtered with a 50-tap 1.5-Hz cutoff filter to remove out-of-band noise. The I and Q signals are then combined by SVD combining [23]. First, any dc offset is removed from the data, and the covariance matrix between the I and Q channels is found. The I and Q data is then projected onto the eigenvector of the covariance matrix with the largest eigenvalue. Details on this technique can be found in [23]. The respiration rate is found by autocorrelating the signal in an 18-s Hamming window and finding the local maxima that indicates a rate between 4–30 breaths/min. The same rate-finding technique is used for the chest and abdominal respiration straps, but the strap signals are combined with equal ratio combining rather than SVD combining, are low-pass filtered after they are combined rather than before, and have their dc offset removed since they do not have dc-offset removal in the analog signal conditioning. Equal-ratio combining involves adding the two sources of data after ensuring they are in phase.

D. Human Subjects

Seven women and 15 men were measured in this study. The age of the subjects ranged from 19 to 67 with a mean age of 34. The body mass index (BMI) of the subjects ranged from 18.3 to 31.4, with a mean BMI of 24.3. The average resting heart rate varied from 43.2 to 93.6 beats/min, with a mean of 70.4 beats/min, and the respiration rates varied from 4.8 to 21.0 breaths/min, with a mean of 12.8 breaths/min. The subject data is listed in Table II.

The subject's body weight was measured on a strain-gauge-based digital scale with clothing on. The chest circumference and waist circumference were measured with a 0.7-cm-wide measuring tape. The subject was instructed to stand erect, with the abdomen relaxed, with his/her feet at shoulder width, and with the arms out enough to allow the passage of the tape around the chest or waist. Once the tape was around the chest or waist, the subject was instructed to lower his/her arms to their natural position at his/her side. The chest circumference was measured in a horizontal plane at the level of the bottom of the sternum. The waist circumference was measured in a horizontal plane at the level of the natural waist or the narrowest part of the torso. If the subject's waist was not well defined, the smallest horizontal circumference between the ribs and iliac crest was measured. Measurements were made at the end of a normal inspiration and at the end of a normal expiration without the tape compressing the skin.

The chest breadth and depth were measured with Lafayette 01440 chest-depth calipers (Lafayette Instrument Company,

TABLE II
MEASURED AND COLLECTED SUBJECT DATA

	Age	Height [cm]	Weight [kg]	BMI [kg/m²]	Chest Breadth [cm]	Chest Depth [cm]	Waist Circumference [cm]	Chest Circumference [cm]	Heart Rate [bpm]	Respiration Rate [rpm]
Average	34.0	174.2	74.6	24.3	27.5	18.7	80.8	86.1	70.4	12.8
Standard Deviation	11.2	9.5	17.4	4.2	3.9	2.9	18.6	12.5	11.4	4.0

The subject's age was reported by the subject. The BMI is the subject's body mass index, calculated as Weight/Height², with the weight in kg and the height in m. The subject's chest breadth, chest depth, waist circumference, and chest circumference were all measured at exhale. The heart rate and respiration rate are the subject's average heart and respiration rates measured in beats per minute and respirations per minute.
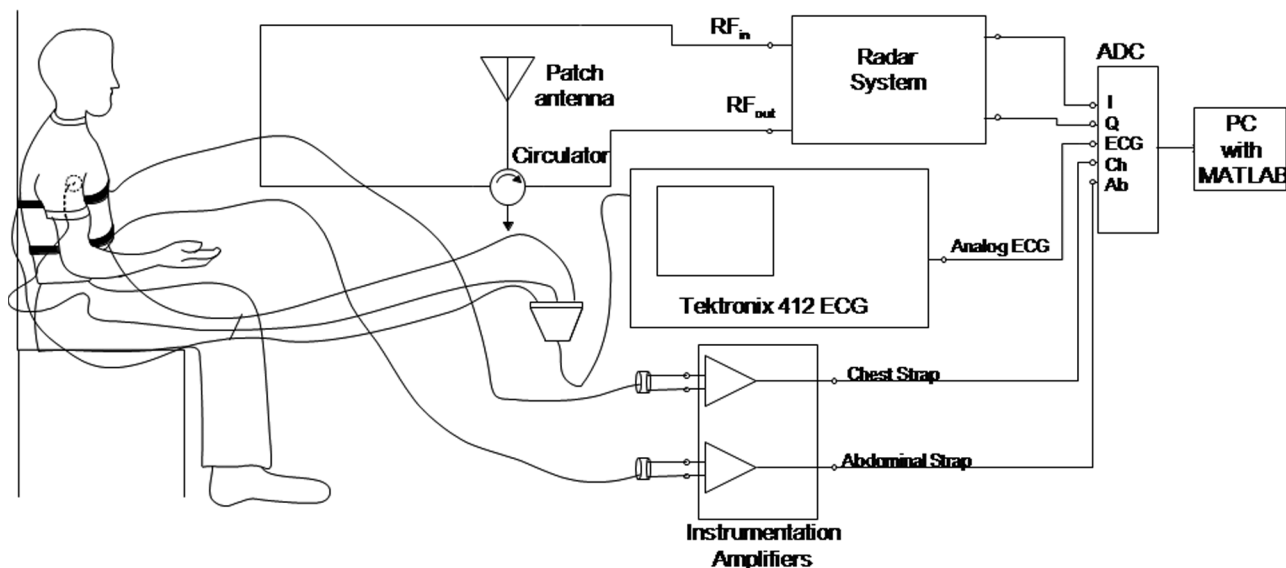
Fig. 3. Human subjects experimental setup. The radar system consists of the radar chip mounted on a printed circuit board and a baseband board. The Tektronix 412 ECG is a three-lead ECG system that has been approved by the Department of Clinical Engineering Stanford University Medical Center, and has an analog output so it can be digitized simultaneously with the control. The chest and abdominal straps are isolated with instrumentation amplifier before they are digitized.

Lafayette, IN). The subject was instructed to stand erect, with the feet at shoulder width. For chest breadth measurements, the arms far enough out to allow access to the measurement site with the calipers, and for chest depth measurements, the arms were at the sides. For chest breadth measurement, the tips of the calipers were placed on the sixth ribs with the measurer's fingers beneath the caliper tips to prevent them from slipping into the intercostal spaces. For chest depth measurement, one tip of the calipers was placed on the sternum in the midline at the level of the fourth cost-sternal junction, and the other time was placed on the spinous process of the vertebra that is in the same horizontal place. Very light pressure was applied and the chest breadth and depth were measured both at the end of a normal inspiration and at the end of a normal expiration.

BMI is used as a proxy for total body fat. This is the most commonly used estimate of body type, largely because weight and height are easy to measure, highly consistent, and require minimal expenditure on equipment. The BMI is calculated as the weight divided by the square of the height.

E. Human Subjects Experimental Procedure

This experiment was performed under Stanford University protocol number 2899, approved by the Stanford University In-

ternal Review Board in August 2005. After obtaining informed consent, the administrator asked the subject whether he/she has any diseases or disorders relating to or affecting the heart or respiratory system, whether he/she has a pacemaker or neurostimulator, and if a female, whether she is pregnant. If the subject answered yes to any of these questions, he/she would have been excluded from the study, but no exclusions were necessary. Each subject was given a new T-shirt to wear for the duration of the measurements if he/she was not already wearing a T-shirt, and was provided with a private area to change into this T-shirt. The administrator of the measurement asked the subject his/her age and gender and then measured the subject's weight, height, and thorax dimensions. The thorax dimensions were measured both at full inhale and full exhale, and included chest circumference, waist circumference, chest breadth, and chest depth.

The experimental setup for the human subjects method comparison is illustrated in Fig. 3. The control sensors for heart and respiration rate were then affixed to the subject. ECG was chosen for heart-rate reference since it is considered the "gold standard" for heart-rate measurements. The ECG electrodes were affixed to the subject's left and right upper arms and left abdomen, and the piezoelectric respiratory effort belts were affixed on the subject's abdomen and chest. The subject was

then asked to sit in a chair for the measurements, and the antenna height was adjusted to be approximately level with the subject's sternum, facing the torso. The subject was asked to refrain from talking and any other motion for the duration of each measurement if possible. Each measurement had a 90-s duration. Two measurements were made at each range; ranges were 0.5, 1.0, 1.5, and 2.0 m. The subject's chair was not moved and the equipment, all on a cart, was moved to vary the range. The range was measured with a measuring tape from the subject's sternum to the antenna. When the measurements were completed, the subject was instructed to remove the control sensors. The subject was then provided with a private area to change back into his/her shirt if necessary.

The control measurement for the heart rate is a three-lead ECG with LA and RA electrodes affixed to the left and right arms, and the LL electrode affixed to the left side of the abdomen. A Tektronix 412 ECG display and amplifier (Tektronix, Richardson, TX) was used for isolation and signal conditioning; its analog output was digitized simultaneously with the Doppler signal. Commercially available FDA-approved button-style ECG electrodes were used.

The control measurements for respiration were made with Dymedix piezoelectric respiratory effort straps (Dymedix, Minneapolis, MN). The straps were connected to a signal conditioning circuit of instrumentation amplifiers.

F. Calculation of SNR

The SNR of the heart signal is calculated from the power spectral density of the Doppler signal. The average rate of the ECG signal is determined to be the center of the signal, and the power within 10 beats/min of the center is considered to be the signal power, with all power outside this window considered to be the noise power. The same technique is used for the respiration, but the signal is the power within 6 breaths/min of the rate from the belts, and if the rate is below 6 breaths/min, the minimum rate is 0.1 breaths/min and the maximum rate is 12.1 breaths/min. The respiration signal's signal power is corrected for the amount of the signal that is removed by the baseband dc-blocking filter by dividing the SNR by the gain of the filter.

G. Bland-Altman Analysis for Method Comparison Studies

The Bland-Altman analysis technique for method comparison involves plotting the difference between the two methods' measurement values against the average of the two measurements [25]. In this case, Doppler radar results were compared with those obtained from references, ECG for heart rate, and respiratory effort belt for respiratory rate. The mean difference is then an estimate of the average bias of one method relative to the other. Assuming the measurement error has a Gaussian distribution about the bias, the 95% confidence intervals can be calculated as the bias ± 1.96 times the standard deviation of the differences. The bias is calculated as the mean of the difference between the two measurements. The Bland-Altman statistics are calculated for 60 s from each measurement, starting after 22 s, so that the filters and exponential average have time to load.

IV. RESULTS

The phase noise of the CMOS oscillator was measured using the delay line/mixer frequency discriminator method with the Agilent E5500 phase-noise measurement system. The single-sideband phase noise at a 1-Hz offset frequency is $+64 \pm 1.6$ dB/Hz ($N = 3$). The delay from the RF output to the antenna and the antenna to the RF input was measured to be 5 ns. The cutoff frequency of the antialiasing filter is 21 Hz. The dc-blocking cutoff frequency is 0.23 Hz, and the gain is 40 dB.

A. Heart and Respiration Signals and Rates

The signatures and rates collected from subject 4062 at ranges of 0.5 and 1.5 m is shown in Figs. 4 and 5, respectively. For each range, the 60-s traces that were used for Bland-Altman rate comparison are shown. These traces are the combined I and Q heart and respiration signals from the Doppler radar, the ECG signal, and the combined chest and abdomen respiratory effort straps. This subject was chosen because his low heart rate (average 46 beats/min) make the heart signal easier for the reader to view, and because the 31-year-old male's body shape and size were not at the extremes of this subject population in any dimension.

The mean and standard deviation of the difference between the heart or respiration rates and the 95% confidence interval at each range found with the Doppler system and the control are shown in Table III. Bland-Altman plots for all subjects are shown in Fig. 6(a)–(e) for heart rates at 0.5 m, heart rates at 1.0 m, heart rates at 1.5 m, respiration rates at 1.0 m, and respiration rates at 2.0 m, respectively.

B. SNR

The SNR was calculated for the heart and respiration traces for each subject for each range. The average SNRs at each range for heart and respiration are shown in Table IV and Fig. 7.

The correlation coefficient was calculated between each measured parameter and the calculated SNR at each range. The heart SNR did not show statistically significant correlation with any of the measured parameters, but the respiration SNR had significant correlations with chest circumference, waist circumference, chest depth, and height-waist circumference product at 0.5, 1.0, and 1.5 m. The correlation coefficient and its associated p value are shown for each of these parameters in Table V.

V. DISCUSSION

With the accuracy measured in this application, the current Doppler radar system could be used in applications where a normal versus abnormal heart rate needs to be detected at ranges up to 1.0 m, but it is not sufficiently reliable for heart-rate measurements at ranges beyond 1 m. The respiration is reliable to 1.5 m, and becomes less reliable at 2.0 m.

Some subjects were less still than others, and the detected motion interfered with the extraction of the heart and respiration rates. Three subjects had motion noted by the experiment administrator. This most likely further decreased the accuracy of these measurements. While multiple antenna systems [6], [7] and advanced signal processing [26] have been explored to overcome this limitation, random motion is still a challenging issue beyond the scope of this paper.
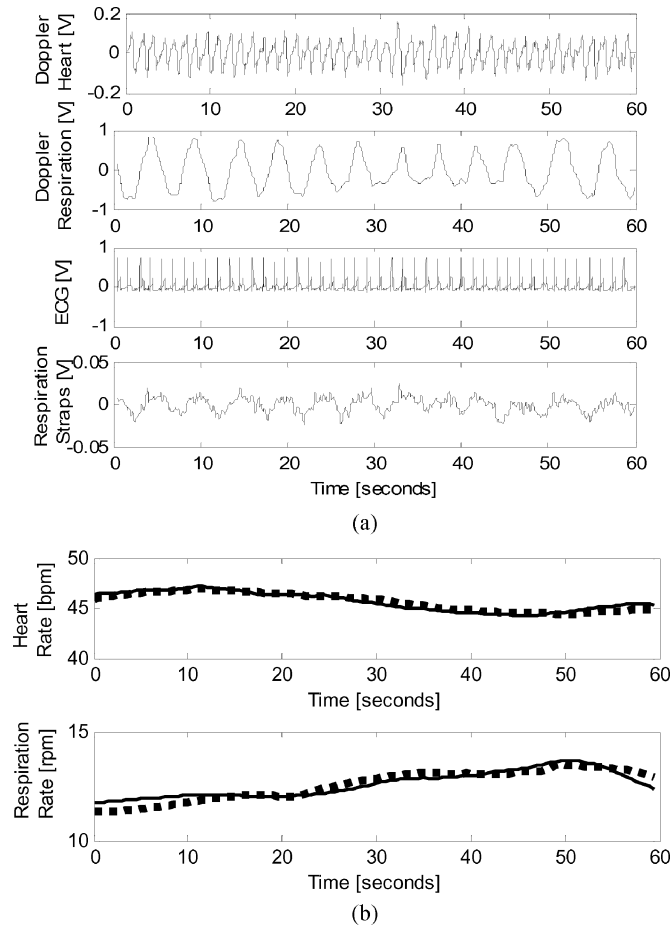
Fig. 4. (a) Heart and respiration signatures and (b) rates measured on subject 4062 at 0.5 m. In the signatures plot, the top trace is the heart motion signature obtained with the Doppler radar system, the second trace is the respiration motion signature obtained with the Doppler radar, the third trace is the ECG, and the bottom trace is the heart motion trace obtained with the respiratory effort belts. In the rates plot, the dotted line is the rate obtained with the control (ECG or respiratory effort belts) and the solid line is that obtained with the Doppler radar system.
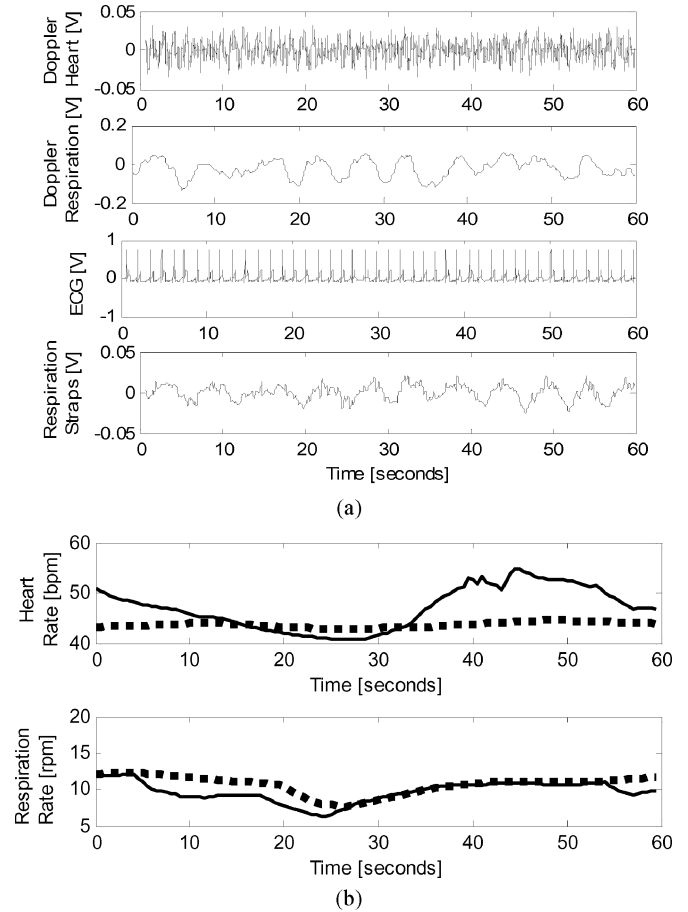

Fig. 5. (a) Heart and respiration signatures and (b) rates measured on subject 4062 at 1.5 m. In the signatures plot, the top trace is the heart motion signature obtained with the Doppler radar system, the second trace is the respiration motion signature obtained with the Doppler radar, the third trace is the ECG, and the bottom trace is the heart motion trace obtained with the respiratory effort belts. In the rates plot, the dotted line is the rate obtained with the control (ECG or respiratory effort belts) and the solid line is that obtained with the Doppler radar system.

The heart and respiration SNR versus range data shown in Fig. 7 matches much more closely with the residual phase noise model than the other noise model, indicating that residual phase noise is the dominant noise source, as was predicted.

Significant variation of the SNR of the heart signal with any of the measured parameters was not detected. It was expected that age or BMI could affect the heart signal, as arterial compliance decreases with increasing age and fat could attenuate the amount of motion at the skin–air interface. However, no significant correlations between the heart SNR and age or BMI were seen. Note that in Fig. 7 the standard error of the SNR for the heart measurement decreases with increasing range. This is because as the SNR is increasingly dominated by noise, the physiological variations between the subjects have less of an effect.

Respiration SNR was not expected to be significantly affected by age or by the BMI, except as much as a larger body mass index leads to an increase in chest dimensions. The respiration SNR was expected to be affected by the chest dimensions of the subject since the theoretical SNR equation is linear with the RCS of the target, and the RCS of the part of the chest that moves

TABLE III
BLAND-ALTMAN DATA FOR HEART RATE AND RESPIRATORY
RATE MEASUREMENTS AT EACH RANGE

	Range	95% Confidence Interval	Mean	Standard Deviation
Heart Rate	0.5 m	+7.04/-7.00	0.02	3.58
	1.0 m	+11.18/-9.59	0.80	5.30
	1.5 m	+19.74/-16.74	1.50	9.31
	2.0 m	+25.9/-16.15	4.88	10.73
Respiratory Rate	0.5 m	+4.75/-4.01	0.37	2.23
	1.0 m	+4.32/14.78	-0.23	2.32
	1.5 m	+4.44/-5.06	-0.31	2.42
	2.0 m	+7.12/-10.53	-1.70	4.50

with respiration increases with the size of the subject. The respiration SNR was positively correlated with all size-related variables, and statistically significantly correlated with chest circumference, waist circumference, and chest depth.
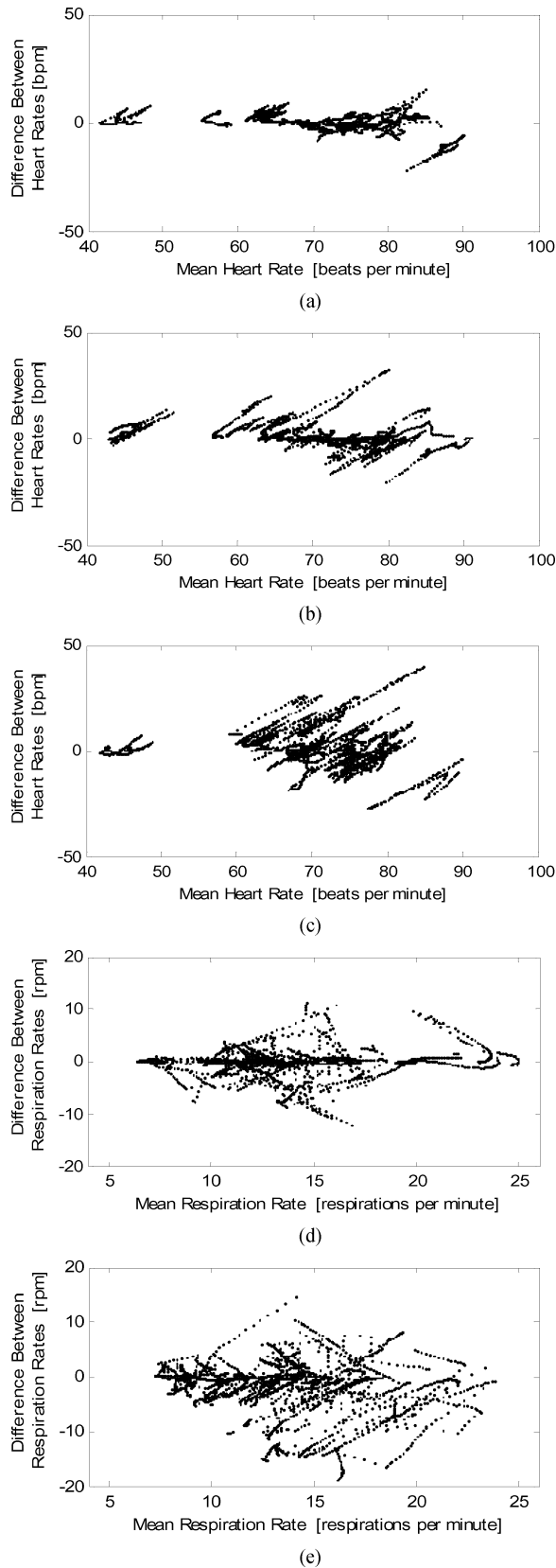
Fig. 6. Bland-Altman plots for all subjects. Heart rates at: (a) 0.5 m, (b) heart rates at 1.0 m, (c) heart rates at 1.5 m, (d) respiration rates at 1.0 m, and (e) respiration rates at 2.0 m.

	Range	Average SNR	Average SNR [dB]
Heart	0.5 m	1.07 ± 0.83	0.29 ±
	1.0 m	0.49 ± 0.22	-3.10 ±
	1.5 m	0.24 ± 0.18	-6.20 ±
	2.0 m	0.17 ± 0.06	-7.70 ±
Respiration	0.5 m	31.61 ± 10.13	15.00 ± 1.08
	1.0 m	19.16 ± 5.49	12.82 ± 1.05
	1.5 m	11.00 ± 1.95	10.41 ± 0.77
	2.0 m	10.95 ± 3.80	10.39 ± 1.23
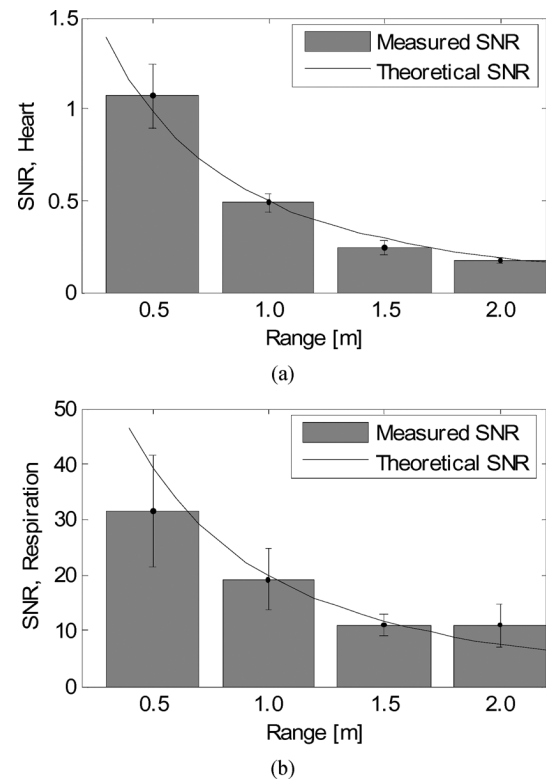
Fig. 7. Measured SNR versus range for: (a) heart and (b) respiration measurements. Error bars show standard error.

and respiration, and these values can be used in future assessments of similar systems. Based on system parameters from Table I, the RCS–MSM product was calculated to be 250 mm^4 for respiratory motion, and 2.25 mm^4 for heart motion. Thus, the respiratory RCS–MSM product was found to be 110 times that of the heart signal.

The error was plotted as a function of the SNR for all measurements in Fig. 8. When the SNR is plotted in decibels, there is an approximately linear relationship so the accuracy is proportional to the log of the SNR. The model for heart accounts for 59% of the variation in heart, and the model for respiration accounts for 42% of the variation in respiration. This indicates

If the measured variables are input into the predicted SNR equation, the RCS–MSM product can be calculated for the heart

TABLE V
CORRELATION BETWEEN RESPIRATION SNR AND
BODY MEASUREMENTS AT EACH RANGE

Range	Chest Circ.		Waist Circ.		Chest Depth		Height-Waist Circ. Product	
	r	p	r	p	r	p	r	p
0.5 m	0.36	0.10	0.40	0.06	0.40	0.07	0.36	0.10
1.0 m	0.53	0.01	0.43	0.05	0.55	0.01	0.42	0.05
1.5 m	0.48	0.02	0.44	0.04	0.67	0.00	0.43	0.05
2.0 m	0.28	0.21	0.23	0.30	0.23	0.30	0.27	0.21
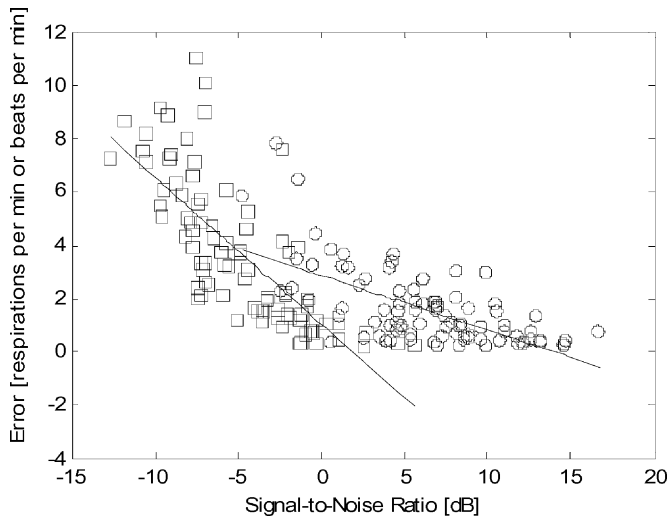
Fig. 8. SNR and error. The error is defined as the standard deviation of the difference between the control and Doppler radar measurement. The squares indicate the heart data, the bold line indicates the best fit line for the heart data, the circles indicate the respiration data and the thin line indicates the best fit for the respiration data.

that the SNR does affect the ability to detect heart and respiration rates. The accuracy was sometimes very good with an SNR as low as -1 dB, but it was not consistently good until the SNR was greater than 10 dB. This indicates that improvements in the SNR will improve the accuracy for rate finding. This also indicates that with better signal processing, the accuracy could be improved for signals with SNR as low as -1 dB.

The SNR could be improved by decreasing the residual phase noise, and the accuracy could be improved by using more advanced signal processing so that the rates can be found accurately at lower SNRs. The addition of a low-noise amplifier at the front end will not improve the SNR, as the limiting noise source is the residual phase noise. Alternatively, these techniques could be used to extend the current accuracy to a greater range.

With the single chip version of the device, residual phase noise is the dominant noise source, and by improving the oscillator phase noise, the SNR could be improved. One way to reduce the residual phase noise is to reduce the RF phase noise of the source. This could be accomplished by fabricating a chip with a technology other than CMOS for the oscillator, using higher quality factor passive elements (possibly off-chip), or by phase locking the CMOS oscillator to a low phase-noise reference. Another way to reduce the residual phase noise is to minimize the delay between the transmitter and antenna and between the antenna and receiver. The 5-ns delay in this system is equivalent to a 75-cm increase in the range. If the circulator and antenna were placed on the same board as the radar chip, this delay could be reduced to as low as 1 ns, or an effective range of 15 cm. This 4-ns improvement would theoretically allow measurements to be made at 50 cm further with similar results.

VI. CONCLUSION

The CMOS-based Doppler radar system was effective at measuring heart rate up to a range of 1 m and measuring respiration up to a range of 1.5 m. Theoretical SNR derivation for Doppler radar heart and respiration rate monitor was validated using data obtained on 22 human subjects. It was found the respiratory SNR was only about ten times higher than for the heart. Measurement error was analyzed as a function of SNR. It was found that the accuracy was sometimes very good with an SNR as low as -1 dB, but it was not consistently good until the SNR was greater than 10 dB. This indicates that improvements in the SNR will improve the accuracy for rate finding.

REFERENCES

[1] J. C. Lin, "Microwave sensing of physiological movement and volume change: A review," *Bioelectromagnetics*, vol. 13, no. 6, pp. 557–565, 1992.

[2] E. M. Staderini, "UWB radars in medicine," *IEEE Aerosp. Electron. Syst. Mag.*, pp. 13–18, Jan. 2002.

[3] B. K. Park, V. M. Lubecke, and O. Boric-Lubecke, "Arctangent demodulation in quadrature Doppler radar receiver system with DC offset compensation," *IEEE Trans. Microw. Theory Tech.*, vol. 55, no. 5, pp. 1073–1079, May 2007.

[4] A. Host-Madsen, N. Petrochilos, O. Boric-Lubecke, V. M. Lubecke, B. K. Park, and Q. Zhou, "Signal processing methods for Doppler radar heart rate monitoring," in *Signal Processing Techniques for Knowledge Extraction and Information Fusion*, D. Mic, Ed. *et al.* Berlin, Germany: Springer-Verlag, 2008.

[5] H. J. Kim, K. H. Kim, Y. S. Hong, and J. J. Choi, "Measurement of human heartbeat and respiration signals using phase detection radar," *Rev. Sci. Instrum.*, vol. 78, pp. 104703-1–104703-3, 2007.

[6] C. Li and J. Lin, "Complex signal demodulation and random body movement cancellation techniques for non-contact vital sign detection," in *IEEE MTT-S Int. Microw. Symp. Dig.*, Atlanta, GA, Jun. 2008, pp. 567–570.

[7] R. Fletcher and J. Han, "Low-cost differential front-end for Doppler radar vital signs monitoring," in *IEEE MTT-S Int. Microw. Symp. Dig.*, Boston, MA, Jun. 2009, pp. 1325–1328.

[8] J. Oum, D. Kim, and S. Hong, "Two frequency radar sensor for non-contact vital sign monitor," in *IEEE MTT-S Int. Microw. Symp. Dig.*, Atlanta, GA, Jun. 2008, pp. 919–922.

[9] A. Droitcour, V. Lubecke, J. Lin, and O. Boric-Lubecke, "A microwave radio for Doppler radar sensing of vital signs," in *IEEE MTT-S Int. Microw. Symp. Dig.*, Phoenix, AZ, May 2001, pp. 175–178.

[10] H. J. Kim, K. H. Kim, Y. S. Hong, and J. J. Choi, "Measurement of human heartbeat and respiration signals using phase detection radar," *Rev. Sci. Instrum.*, vol. 78, pp. 104703-1–104703-3, 2007.

[11] A. D. Droitcour, O. Boric-Lubecke, V. Lubecke, J. Lin, and G. T. A. Kovacs, "0.25 μm CMOS and BiCMOS single-chip direct-conversion Doppler radars for remote sensing of vital signs," in *Int. Solid-State Circuits Conf. Dig.*, 2002, vol. 1, pp. 348–349.

[12] A. D. Droitcour, O. Boric-Lubecke, V. M. Lubecke, J. Lin, and G. T. A. Kovacs, "Range correlation and I/Q performance benefits in single-chip silicon Doppler radars for noncontact cardiopulmonary monitoring," *IEEE Trans. Microw. Theory Tech.*, vol. 52, no. 3, pp. 838–848, Mar. 2004.

[13] A. D. Droitcour, O. Boric-Lubecke, V. M. Lubecke, J. Lin, and G. T. A. Kovacs, "Chest motion sensing with modified silicon base station chips," *IEICE Trans. Electron.*, vol. E87-C, no. 9, pp. 1524–1531, 2004.

[14] C. Lee, Y. Xiao, and J. Lin, "A 5 GHz double-sideband radar sensor chip in 0.18 μm CMOS for noncontact vital sign detection," *IEEE Microw. Wireless Compon. Lett.*, vol. 18, no. 7, pp. 494–496, Jul. 2008.

[15] P. B. Colditz, K. R. Dunster, G. J. Joy, and I. M. Robertson, "Anetoderma of prematurity in association with electrocardiographic electrodes," *J. Amer. Acad. Dermatol.*, vol. 41, no. 3, pp. 479–481, 1999.

[16] S. Loo, T. Kuo, G. Waters, M. Muller, and T. L. H. Brown, "A mobile electrode for ECG monitoring," *Burns*, vol. 30, no. 2, p. 203, 2004.

[17] "Code of federal regulations, title 47: Telecommunications, part 15: Radio frequency devices," FCC, Washington, DC, 2000.

[18] M. C. Budge, Jr. and M. P. Burt, "Range correlation effects on phase and amplitude noise," in *Proc. IEEE Southeastcon*, 1993, 5 pp.

[19] M. I. Skolnik, "An introduction to radar," in *Radar Handbook*, M. I. Skolnik, Ed. San Francisco, CA: McGraw-Hill, 1990, pp. 1.1–1.21.

[20] T. Kondo, T. Uhlig, P. Pemberton, and P. D. Sly, "Laser monitoring of chest wall displacement," *Eur. Respiratory J.*, vol. 10, pp. 1865–1869, 1997.

[21] A. DeGroote, M. Wantier, G. Cheron, M. Estenne, and M. Pavia, "Chest wall motion during tidal breathing," *J. Appl. Physiol.*, vol. 83, no. 5, pp. 1531–1537, 1997.

[22] G. Ramachandran and M. Singh, "Three-dimensional reconstruction of cardiac displacement patterns on the chest wall during the P, QRS, and T-segments of the ECG by laser speckle interferometry," *Med. Biol. Eng. Comput.*, vol. 27, no. 5, pp. 525–530, 1989.

[23] I. T. Jollife, *Principal Component Analysis*. New York: Springer-Verlag, 2002.

[24] C. Li, C. Zheng, and C. Tai, "Detection of ECG characteristic points using wavelet transforms," *IEEE Trans. Biomed. Eng.*, vol. 42, no. 1, pp. 21–28, Jan. 1995.

[25] J. M. Bland and D. G. Altman, "Statistical methods for assessing agreement between two methods of clinical measurement," *Lancet*, vol. 1, no. 8476, pp. 307–310, 1986.

[26] I. Mostafanezhad, O. Boric-Lubecke, V. Lubecke, and A. Host-Madsen, "Cancellation of unwanted motion in a handheld Doppler radar used for non-contact life sign monitoring," in *IEEE MTT-S Int. Microw. Symp. Dig.*, Jun. 2008, pp. 1171–1174.

[27] I. Mostafanezhad, O. Boric-Lubecke, V. Lubecke, and D. Mandic, "Application of empirical mode decomposition in removing fidgeting interference in Doppler radar life signs monitoring devices," in *IEEE EMBC09*, Sep. 2009, pp. 340–343.

Amy D. Droitcour (S'98–M'00) received the B.S. degree in electrical engineering (*cum laude*) (with honors) from Cornell University, Ithaca, NY, in 2000, and the M.S. and Ph.D. degrees in electrical engineering from Stanford University, Stanford, CA, in 2003 and 2006, respectively.

She is currently the Chief Technology Officer with Kai Sensors, Honolulu, HI, where she directs the development the company's portfolio of products, as well as the company's regulatory and clinical affairs.

Dr. Droitcour was the recipient of the Lucent Technologies/Bell Laboratories Graduation Research Fellowship. She received an honorable mention at the 2001 IEEE MTT-S International Microwave Symposium (IMS) Student Paper Competition, and was the first place recipient of the 2003 IEEE MTT-S IMS competition. She was also the recipient of the IEEE MTT-S Fellowship in 2004.

Olga Boric-Lubecke (S'90–M'90–SM'01) received the B.Sc. degree from the University of Belgrade, Belgrade, Yugoslavia, in 1989, the M.S. degree from the California Institute of Technology, Pasadena, in 1990, and the Ph.D. degree from the University of California at Los Angeles (UCLA), in 1995, all in electrical engineering.

She is currently with the Department of Electrical Engineering, University of Hawaii at Manoa, Honolulu, HI. She cofounded the startup company Kai Sensors, Honolulu, HI.

Dr. Boric-Lubecke serves on the Technical Program Committee and Steering Committee for various IEEE and SPIE symposia. She has coauthored papers that were selected for Honorable Mention at the 2001 IEEE Microwave Theory and Techniques Society (IEEE MTT-S) International Microwave Symposium (IMS), Third Place at the 2001 EMBS, First Place at the 2003 IEEE MTT-S IMS, and competition finalist at the 2006 RWS. She was a corecipient of the Emerging Technology Award presented at TechConnect 2007.

Gregory T. A. Kovacs (S'82–M'91–SM'06–F'09) received the BA.Sc. degree in electrical engineering from the University of British Columbia, Victoria, BC, Canada, in 1984, the M.S. degree in bioengineering from the University of California at Berkeley, in 1985, and the Ph.D. degree in electrical engineering and MD degree from Stanford University, Stanford, CA, in 1992, respectively.

He possesses extensive industry experience including cofounding several companies. He is a Professor of electrical engineering with Stanford University along with a courtesy appointment with the Department of Medicine. In addition, he is the Director of the Microsystems Technology Office, Defense Advanced Research Projects Agency (DARPA). He held the Noyce Family Chair and was a Terman and then University Fellow with Stanford University. His current research interests include biomedical instruments and sensors, miniaturized spaceflight hardware, and biotechnology.

Dr. Kovacs is a long-standing member of the Defense Sciences Research Council (DARPA) and has served as an associate chair and chairman. He is a Fellow of the American Institute for Medical and Biological Engineering. He was the recipient of a National Science Foundation (NSF) Young Investigator Award.